Jurnal Kejuruteraan 34(1) 2022: 73-87
https://doi.org/10.17576/jkukm-2022-34(1)-07

Perforated Composite Plate Girders with Intermediate Inclined Stiffeners Subjected to Combined Shear and Bending

Mohd Eizlan Majuk[a], Mohd Reza Azmi[a*], Mohd Yazmil Md Yatim[a], Irfana Kabir Ahmad[a] & M. Mukhlisin[b]

[a]*Department of Civil Engineering, Universiti Kebangsaan Malaysia 43600 UKM Bangi, Selangor, Malaysia.*
[b]*Department of Civil Engineering, Politeknik Negeri Semarang 50275 Semarang, Indonesia*

**Corresponding author: mohdreza@ukm.edu.my*

Received 18 April 2021, Received in revised form 12 July 2021
Accepted 13 August 2021, Available online 30 January 2022

ABSTRACT

This paper discusses the ultimate strength of composite plate girders with intermediate inclined stiffeners. The inclination angle of intermediate stiffener, web opening size and span length are the key factors influencing the performance of the composite plate girder. This study used the LUSAS software to develop 20 non-linear finite element models using intermediate stiffener different inclination angles, web opening sizes and span lengths. The intermediate stiffener have an inclination angle of 90°, 75°, 60°, 45° and 30°. The web plates were divided into six or eight sub-panel webs depending on the span length using the intermediate inclined stiffener. The ultimate strength and behaviour of the composite plates are influenced by the inclination angle of the intermediate stiffener, web opening size and span length. Generally, the ultimate strength of the composite plate girder increased when the inclination angle was reduced from 90° to 30° with a corresponding reduction in the web opening size and span length. The increase in the ultimate strength are 44.63% for the web plate with do = 100 mm and L = 3450 mm, 20.41% for the web plate with do = 200 mm and L = 4500 mm, 216.41% for the web plate with do = 100 mm and L = 3450 mm, and 58.89% for the web plate with do = 200 mm and L = 4500 mm due to the formation of tension field on the web panels. The width of the tension field in the plastic hinge increased and shifted depending on the top and bottom flange when using the intermediate inclined stiffener. The composite plate girder with a small web opening of do = 100 mm exhibited a high ultimate strength. The ultimate strength of the composite plate girder with a 60° inclined intermediate stiffener is higher than the intermediate stiffener with a 75° inclination angle. Therefore, the composite plate girder with an inclined intermediate stiffener has a higher ultimate strength.

Keywords: Composite plate girder; intermediate inclined stiffener; web opening size; shear and bending; finite element modelling

INTRODUCTION

In civil engineering, steel plate girders are used to support the applied longitudinal loading. A built-up girder might be used when a hot-rolled steel I-beam is insufficient to resist the high shear loading and bending moment over a long span. The built-up girder is geometrically similar to the steel I-beam sections and resists the bending moment with their flanges while the web panels carry the shear stresses (Darehshouri et al. 2013).

The slender web panel can resist the shear force and achieve the distance between the top and bottom flanges. The flanges resist the internal shear force through the effect of bending moment. The critical factors in the design of steel plate girder the width of tension field action occurred in the web plate gives main contribution of load carrying capacity (Yatim et al. 2020). The slender web plate is likely to undergo local buckling and bend soon after load application. The transverse and longitudinal stiffeners are used to prevent buckling and torsion on the flange section. The longitudinal stiffener divides the web plate into individual sub-panels that increase the stability of the web panel. Evans et al. (1978) and Alinia and Moosavi (2008) have determined the dimensions, numbers and position of the longitudinal stiffener on the web panel that gives optimum steel plate girder performance.

The composite action between the steel plate girder and concrete slab ensures a cost-effective construction without compromising performance (Gavare et al. 2018). These materials are effectively connected with a shear stud. The ultimate and effective composite interaction is achieved when the shear stud resists the relative motion and vertical separation between each connected component (Yatim et al. 2015). The difference in the tension field on the web plate due to the composite action has a beneficial impact on the composite girder ultimate load analysis (Baskar and Shanmugam 2003).

The opening on web plate often seen in a composite girder is for inspection purpose and services passage (Xiao et al. 2018). However, the opening reduces the girder's ultimate strength capacity. Yatim et al. (2017) have shown that the opening reduces the plate girder's ultimate strength, redistribution of stress and structural discontinuity.

Conventional stiffeners are in the transverse and longitudinal directions. However, the intermediate stiffener could be horizontal, longitudinal or inclined. The inclined intermediate stiffener restores the ultimate load capacity of the girder (Guarnieri 1985), (Pritykin & Kirillov 2015), (Azmi et al. 2017) and (Yuan et al. 2019). Azmi et al. (2017) have shown that reducing the inclination angle could increase the ultimate strength of the girder by up to 38%, which is one of the requirements in present-day construction. The utilization of this type of stiffener makes the analysis more complex because the web panel is divided into sub-panels with varying lengths of the sub-panels at the top corner and bottom flange (Ellobody et al. 2017).

In this research, the strength of the composite girder is influenced by the steel plate girder, concrete slab and shear stud (Yatim et al. 2015). The investigation focuses on the inclination angle of the stiffeners, opening size and span length, and used a non-linear finite element by employing the finite element software package.

METHODOLOGY

FINITE ELEMENT MODEL

This research used the LUSAS software package to develop the three-dimension finite element models and performed the non-linear analysis using twenty models of the composite girders. Each model was classified based on the inclination angle of the stiffener, opening size and span length. This research modified the CPG7 girder in the study by Baskar and Shanmugam (2003) to achieve the objective of this study.

The material properties of the steel plate girder and concrete slab were based on the study by Baskar and Shanmugam (2003). Each stiffener is placed at the mid-span of the web plate to divide the thin web into four composite girder panels used for validation purposes. The vertical stiffener in the mid-span prevents premature failure due to local buckling as soon as the load is imposed. Table 1 shows the values of the mechanical properties of the materials used to validate the composite girder. In the table, Es and Ec are the Young's Modulus of the steel and concrete, fy(avg) is the average yield stress for the steel, fcu is the cube compressive strength, and ft is the split tensile strength. These values are used in the simulation of the actual properties of the composite girders.

TABLE 1. The values of the mechanical properties of the steel and concrete materials used for validation

E_s (GPa)	E_c (GPa)	$F_{y(avg)}$ (MPa)	f_{cu} (MPa)	f_t (MPa)
200	23.25	275	49.9	3.3

The 90°, 75°, 60°, 45° and 30° inclination angle of all stiffeners in the developed finite element models are based on the study by Azmi et al. (2017). Table 2 shows the values of the mechanical properties of the materials. The flange and stiffener are 10 mm thick, and the web is 2 mm thick. The web plate is 500 mm high, the web panel is 525 mm long, and the flange is 160 mm wide. The opening size of 100 mm and 200 mm represents the web-opening ratio (do/d) and the span length, L, is 3450 mm and 4500 mm.

The concrete slab is 1200 mm x 150 mm. Table 3 show the details of the models in the numerical analysis. CG is the composite girder, and the inclination angles for intermediate inclined stiffener measured from the bottom of the plate girder are 90°, 75°, 60°, 45° and 30°. The circle opening, Cr, is 100 and 200, and 6P and 8P are the panels. Figures 1 and 2 show the typical models in this study.

TABLE 2. The values of the mechanical properties of the steel and concrete materials for models

E_s (GPa)	E_c (GPa)	$F_{y(avg)}$ (MPa)	f_{cu} (MPa)	f_t (MPa)
200.0	30.0	290.0	49.9	4.99

ELEMENT

Several elements are available in the LUSAS element library. It is essential to select an appropriate element because it determines the behaviour of each model. The three-dimension quadrilateral shell elements (QSL8) have four corners and four intermediate nodes for each element used to mesh the geometry of the web, flanges, stiffener and concrete slab. The selected element allows for the second-order and buckling effects in the plated structures.

The formulation of the element took into account the membrane, flexural and transverse shear deformations suitable for thin-wall applications. It is worth noting that the line mesh has to be used before the mesh to ensure the generation of only the four side elements. The line mesh divides the line into several parts. The modelling used a node to node connection and assumed full interaction between the top steel flange and the concrete slab.

MESH

The validation models in this study used a 50 mm x 50 mm regular finite element mesh based on the result of the convergence study by Basher et al. (2009) for determining the optimum elements for obtaining precise solutions in terms of strength and behaviour with acceptable calculations. However, the analyses of all models used a 25 mm x 25 mm mesh to achieve a more precise value. Figure 3 shows the typical mesh used in the analysis.

MATERIAL MODEL

The composite component, namely the concrete slab and steel plate girder, were modelled as isotropic elastic-perfectly plastic materials with a uniaxial stress-strain relationship. Table 4 presents the details of the model dimension for defining the potential stress of the model. The Poisson ratio for the steel and concrete are 0.3 and 0.2. The Von-Mises yielding criteria represent the ductile behaviour of steel material which exhibited a slight volumetric strain, while the Von-Mises variable criterion is for concrete with non-linear characteristics.

BOUNDARY CONDITION AND LOADING

The boundary condition is a simple pinned and roller type support. The pin support for the composite girder was restrained against displacement in the global x, y and z-direction. However, the roller support is free to move along the z-direction. Both types of support were allowed to rotate in all directions. The fixed restrained in the z-direction on the side of all models prevent lateral torsional buckling (LTB). A gradually increasing vertical concentrated load was applied to the model, and the convergence criterion was based on force and displacement. The model used an automatic load increment with Crisfield's arc length control.

TABLE 3. Details of tested composite girder

Girder	Opening diameter, d_o (mm)	d_o/d (mm)	Inclination angle, θ (°)	Span length, L (mm)
CG90-Cr100-6P	100	0.2	90	3450
CG90-Cr100-8P	100	0.2	90	4500
CG90-Cr200-6P	200	0.4	90	3450
CG90-Cr200-8P	200	0.4	90	4500
CG75-Cr100-6P	100	0.2	75	3450
CG75-Cr100-8P	100	0.2	75	4500
CG75-Cr200-6P	200	0.4	75	3450
CG75-Cr200-8P	200	0.4	75	4500
CG60-Cr100-6P	100	0.2	60	3450
CG60-Cr100-8P	100	0.2	60	4500
CG60-Cr200-6P	200	0.4	60	3450
CG60-Cr200-8P	200	0.4	60	4500
CG45-Cr100-6P	100	0.2	45	3450
CG45-Cr100-8P	100	0.2	45	4500
CG45-Cr200-6P	200	0.4	45	3450
CG45-Cr200-8P	200	0.4	45	4500
CG30-Cr100-6P	100	0.2	30	3450
CG30-Cr100-8P	100	0.2	30	4500
CG30-Cr200-6P	200	0.4	30	3450
CG30-Cr200-8P	200	0.4	30	4500

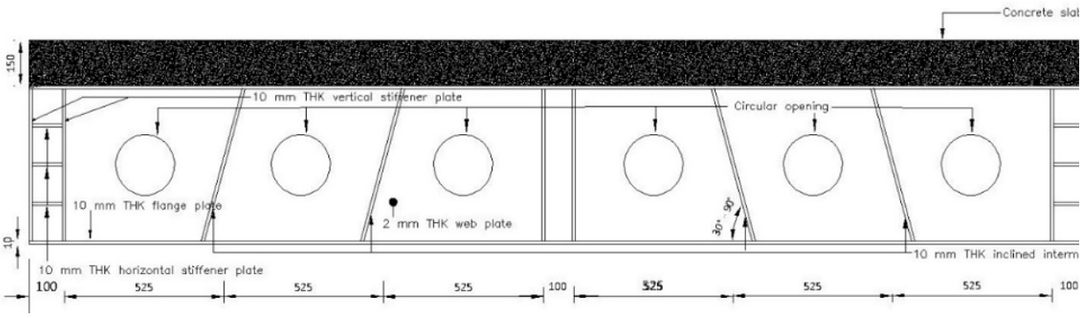

FIGURE 1. Typical section of the 3450 mm plate girder

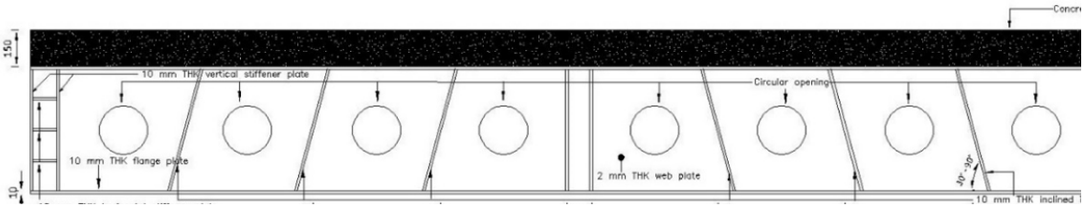

FIGURE 2. Typical section of the 4500 mm plate girder

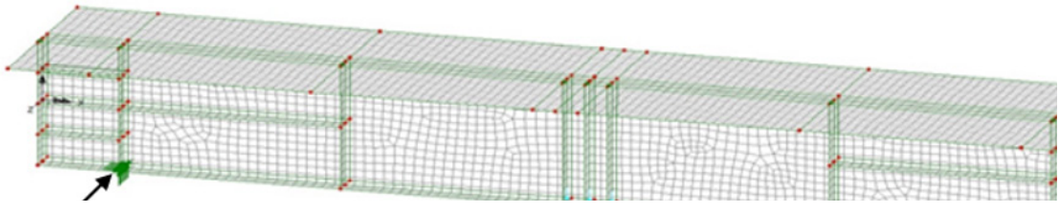

FIGURE 3. Typical finite element mesh

TABLE 4. The ultimate strength of the composite girder with an opening size, do, of 100 mm and span length, L, of 3450 mm

Girder	Inclination angle, θ (°)	d_o/d, (mm)	Ultimate load, $P_{u,FEM}$ (kN)	Percentage of increase in the ultimate load, (%)
CG90-Cr100-6P	90	0.2	424.77	-
CG75-Cr100-6P	75	0.2	470.40	10.74
CG60-Cr100-6P	60	0.2	538.35	26.74
CG45-Cr100-6P	45	0.2	592.56	39.50
CG30-Cr100- 6P	30	0.2	614.33	44.63

TABLE 5. The ultimate strength of the composite girder with an opening size, do, of 100 mm and span length, L, of 4500 mm

Girder	Inclination angle, θ (°)	d_o/d, (mm)	Ultimate load, $P_{u,FEM}$ (kN)	Percentage of increase in the ultimate load, (%)
CG90-Cr100-8P	90	0.2	381.05	-
CG75-Cr100-8P	75	0.2	427.64	12.23
CG60-Cr100-8P	60	0.2	453.99	19.14
CG45-Cr100-8P	45	0.2	455.76	19.61
CG30-Cr100-8P	30	0.2	458.81	20.41

TABLE 6. The ultimate strength of the composite girder with an opening size, do, of 200 mm and span length, L, of 3450 mm

Girder	Inclination angle, θ (°)	d_o/d, (mm)	Ultimate load, $P_{u,FEM}$ (kN)	Percentage of increase in the ultimate load, (%)
CG90-Cr200-6P	90	0.4	186.42	-
CG75-Cr200-6P	75	0.4	204.60	10.00
CG60-Cr200-6P	60	0.4	461.85	147.74
CG45-Cr200-6P	45	0.4	555.49	197.98
CG30-Cr200-6P	30	0.4	589.86	216.41

TABLE 7. The ultimate strength of the composite girder with an opening size, do, of 200 mm and span length, L, of 4500 mm

Girder	Inclination angle, θ (°)	d_o/d, (mm)	Ultimate load, $P_{u,FEM}$ (kN)	Percentage of increase in the ultimate load, (%)
CG90-Cr200-8P	90	0.4	280.26	-
CG75-Cr200-8P	75	0.4	288.54	2.95
CG60-Cr200-8P	60	0.4	419.93	49.84
CG45-Cr200-8P	45	0.4	433.23	54.58
CG-30-Cr200-8P	30	0.4	436.97	55.92

RESULTS AND DISCUSSION

ULTIMATE LOAD CAPACITY AND MODEL ACCURACY

It is essential to verify the model through further analysis. The experimental result for girders CPG7 and CPG8 (Baskar and Shanmugam 2003) were compared to assess their accuracy relative to the finite element predictions. Table 8 shows the accuracy assessment in terms of the ultimate load of the finite element, Pu, and the experimental result, Pu,exp. The Pu/Pu,exp ratio for the finite element and the experimental value is close to the acceptable accuracy of ±10%. Table 4 shows a comparison of the result of the experiment to determine the load-deflection behaviour of CPG7 and CPG8 and the outcome of the finite element analysis using the LUSAS software.

Figure 4 shows the comparison of the load-deflection behavior of girders CPG7 and CPG8 obtained from experimental studies and finite element analysis using LUSAS software. In summary, the proposed modelling method for a finite element can predict the ultimate strength of the composite girder with reasonable accuracy.

TABLE 8. Verification of the numerical model

Girder	LUSAS, $P_{u,FEM}$ (kN)	Experiment, $P_{u,exp}$ (kN)	$P_{u,FEM}/P_{u,exp}$
CPG7	800.67	871	0.92
CPG8	1212.31	1257	0.96

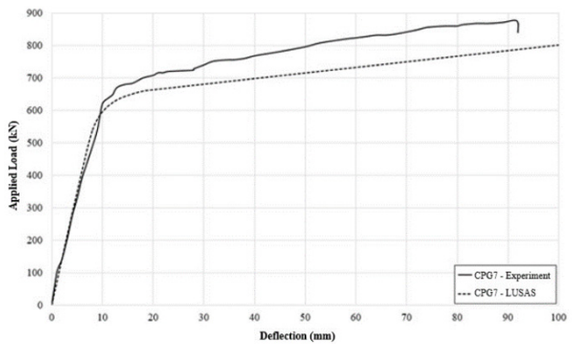

(a) CPG7

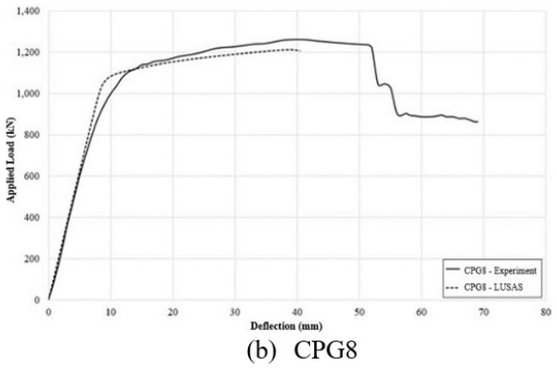

(b) CPG8

FIGURE 4. Comparison of the applied load-deflection behaviour of CPG7 and CPG8.

Tables 6, 7 and 8 show the ultimate load from the numerical analysis, $P_{u,FEM}$, for each girder with the same opening size and span length. Generally, the percentage of the load-carrying capacity increases if the inclination angle of the intermediate stiffener was reduced from $\theta = 90°$ to

30°. The increase in the ultimate strength is 44.63% for the girder with d_o = 100 mm and L = 3450 mm, 20.41% for the girder with d_o = 200 mm and L = 4500 mm, 216.41% for the girder with d_o = 100 mm and L = 3450 mm, and 58.89% for the girder with d_o = 200 mm and L = 4500 mm.

The intermediate inclined stiffener was able to withstand the load imposed on the composite girder by redistributing the force in the web members formed through the positioning of the stiffener. It restored the load carrying-capacity even with the presence of the opening on the web panels. The formation of a web-shaped trapezoid on each panel induced a trusses reaction with smaller inclination angles. The stiffeners increased the width of the tensile field on the trapezoidal web panel, thus giving the web panel the ability to bear higher tensile strengths than the girder with a quadrilateral panel.

The inclined stiffener restored the strength lost by the perforated composite girder. Tables 6 and 7 show a significant difference in the increase in the ultimate strength of the composite girders with an opening of 200 mm and 100 mm. For example, reducing the angle of inclination from 90° to 60° increased the ultimate strength of the girder with d_o= 200 mm and L = 3450 mm by 147.74%, while the ultimate strength of the girder with d_o = 200 mm and L = 4500 mm increased by 49.84%.

The higher ultimate strength is one benefit of using inclined stiffeners as a stiffening element in slender webs. Tables 4, 5, 6 and 7 show that the ultimate load of the girders with a given span length and inclination of the intermediate stiffeners decreased with larger web opening because the reduced

Table 4, 5, 6 and 7 shows the ultimate load capacity of girders with same span length and same inclination angle of intermediate stiffeners will decrease if the size of web openings is larger. The composite girders with a shorter span length and inclination angle of 60° exhibited a greater load-carrying capacity than those with an inclination angle of 75° (Table 4) and those with a longer span length (Table7). In addition, the effect of the shear moment is significant with greater span length because of the low ultimate load capacity. The composite action delayed the failure of the composite girder.

LOAD DEFLECTION RELATIONSHIP

The load-deflection plots were obtained from the finite element analysis in the parametric study. Figures 5(a)-(l) show the behaviour of the composite girders with intermediate stiffeners having the same inclination angle and span length. The curves show the bending behaviour experienced by the composite girders against deflection when applying the load at the mid-span.

Generally, the load-deflection curve is linearly proportional in the early of loading stage. Increasing the applied load resulted in a non-linear curve after reaching the yield point. A further increase in the applied load resulted in a non-linear phase when the composite girder is at its ultimate loading capacity.

The higher tension field band and formation of plastic hinges on the top and bottom of the flange caused a further bending of the web panel. In this post-buckling phase, the composite girder could sustain additional load before failure. The tension band facilitated the achievement of the final load. The benefit of the composite action that increases the tension band is the connection between the concrete slab and steel plate girder.

The load capacity decreased gradually after the ultimate load has been achieved. The web panels with a larger opening have a lower load-carrying capacity, as shown in the load-deflection curve. The composite girder with a small opening of 100 mm has a higher load-deflection curve at the elastic stage than the composite girder with a 200 mm opening. The girders with lower inclination angles exhibited a higher bending stiffness, as shown in the gradient of the curve in the elastic phase. The inclined stiffeners serve as an effective offset for the loss of shear strength in the composite girder.

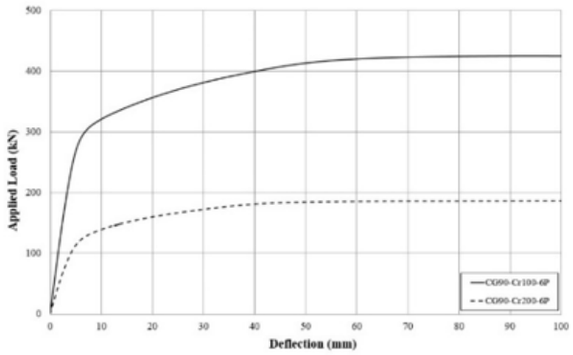

(c) CG90-Cr100-6P and CG90-Cr200-6P

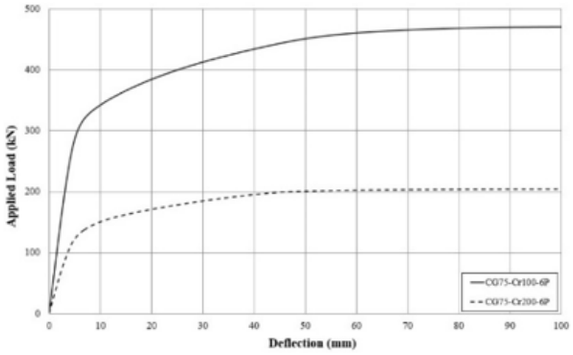

(d) CG75-Cr100-6P and CG75-Cr200-6P

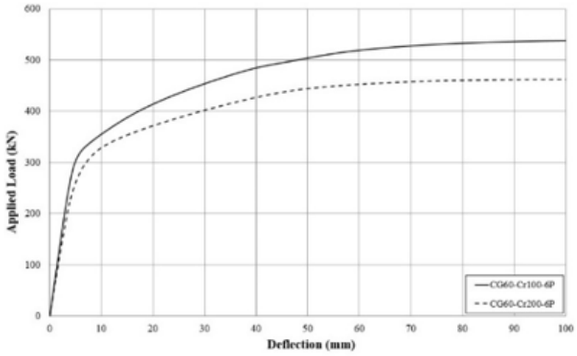

(e) CG60-Cr100-6P and CG60-Cr200-6P

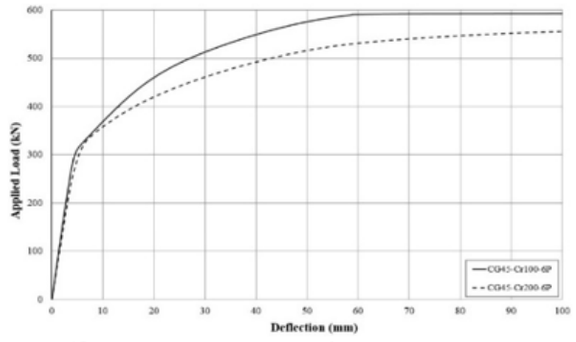

(f) CG45-Cr100-6P and CG45-Cr200-6P

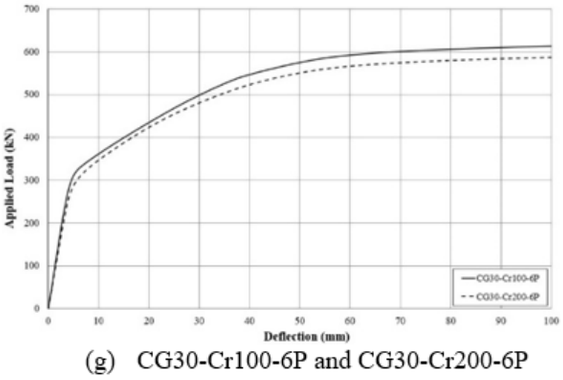

(g) CG30-Cr100-6P and CG30-Cr200-6P

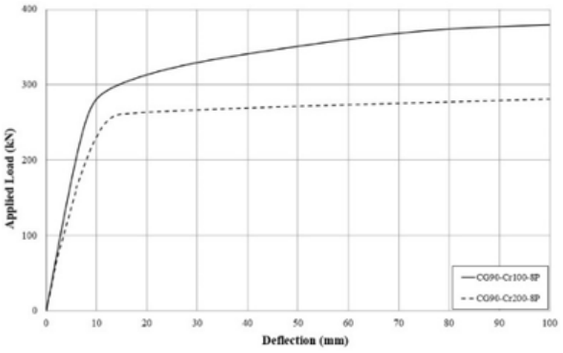

(h) CG90-Cr100-8P and CG90-Cr200-8P

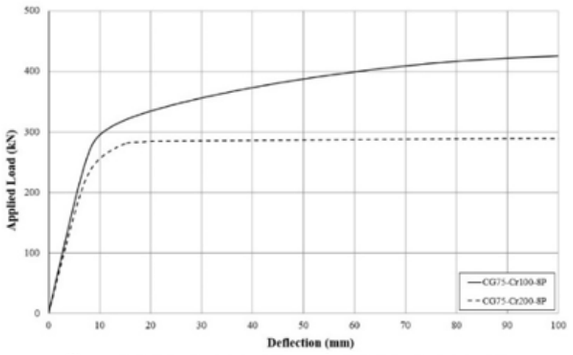

(i) CG75-Cr100-8P and CG75-Cr200-8P

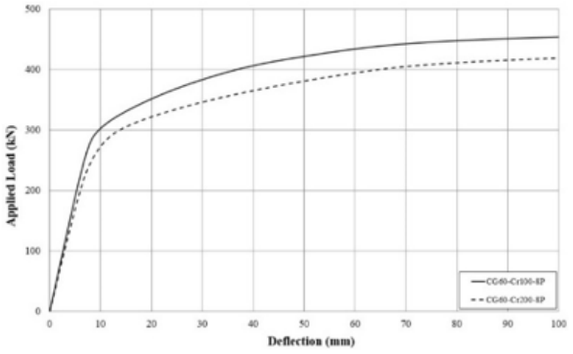

(j) CG60-Cr100-8P and CG60-Cr200-8P

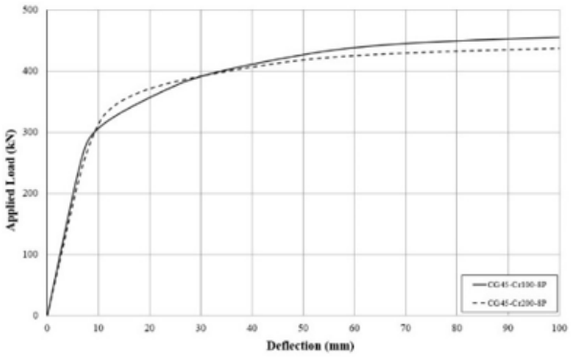

(k) CG45-Cr100-8P and CG45-Cr200-8P

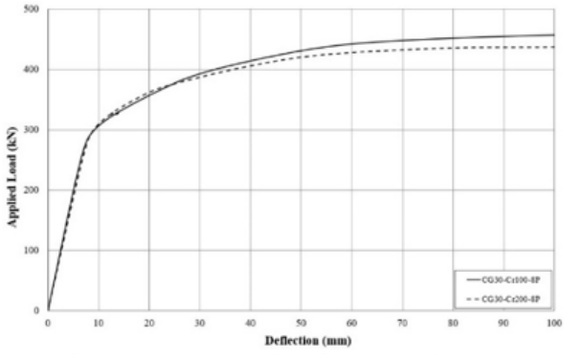

(l) CG30-Cr100-8P and CG30-Cr200-8P

FIGURE 5. The load-deflection response of the composite girders with the same inclination angle, θ, and span length, L, but varying opening size, do

A comparison of the composite girders with the same opening size but different span lengths showed that the bending moment is significant in the girder with a long span. Figures 6(a)-(e) show that the curve for the composite girders with a long span is lower than those with a short span. The composite girders having a long span exhibited a ductile behaviour, where they failed in large bending. The failure is due to the low tensile field generated on the web plates from the composite action in a typical composite girder.

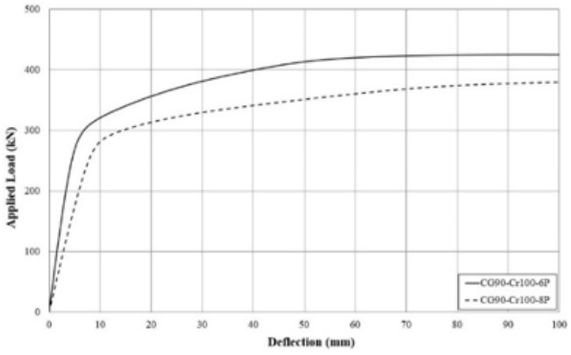

(a) CG90-Cr100-6P and CG90-Cr100-8P

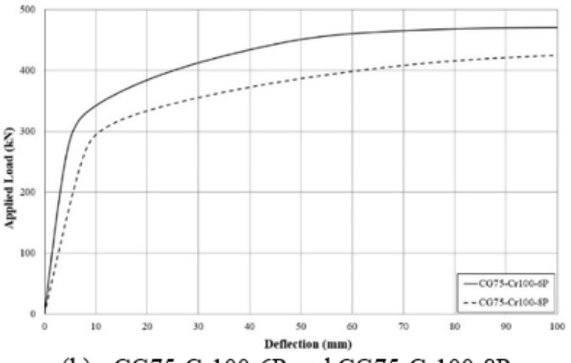

(b) CG75-Cr100-6P and CG75-Cr100-8P

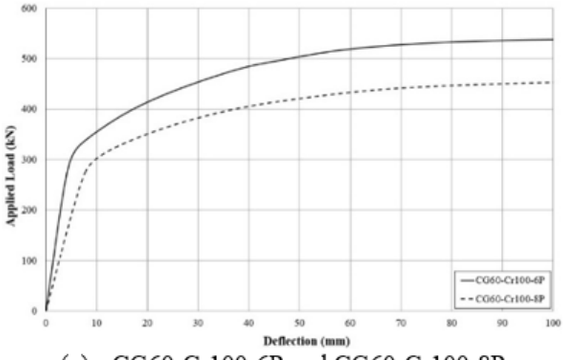

(c) CG60-Cr100-6P and CG60-Cr100-8P

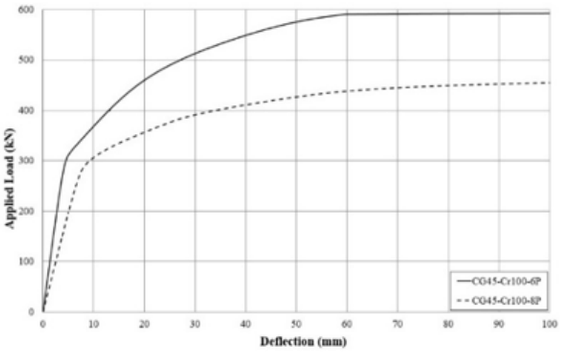

(d) CG45-Cr100-6P and CG45-Cr100-8P

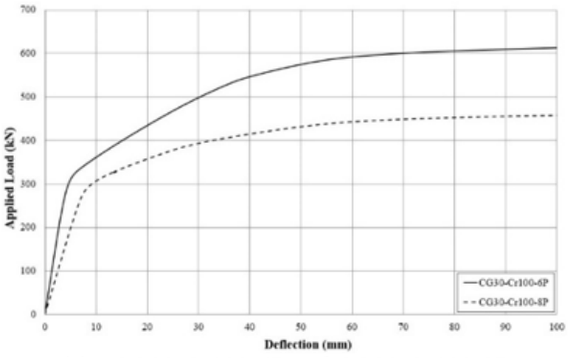

(e) CG30-Cr100-6P and CG30-Cr100-8P

FIGURES 6(a)-(e). The load-deflection responses for the composite girders with the same inclination angle, θ, and opening size, do, but varying span lengths, L

Even though the opening size may influence the ultimate strength of the composite girder, span length has a more considerable impact on the ultimate strength. Figures 7(a)-(h) show that the curves for composite girders with a short span exhibited a higher increment at the elastic stage, which resulted in a higher ultimate strength than those with a long span and greater opening size. The higher ultimate strength could be due to the higher bending moment experienced by the composite girders with a long span. The inclined stiffener was able to sustain the load-carrying capacity even with large opening size. The circular opening did not have a significant impact on the ultimate load compare to the corner opening.

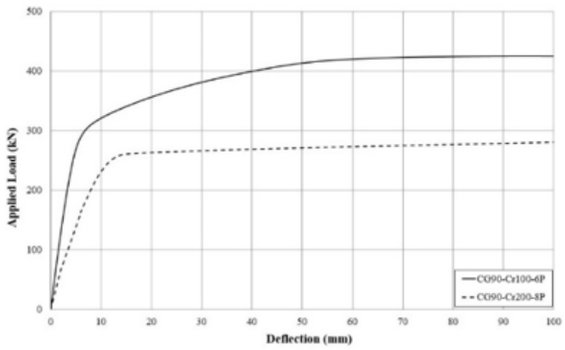

(a) CG90-Cr100-6P and CG90-Cr200-8P

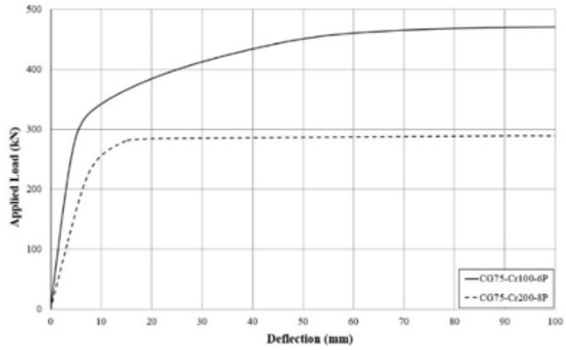

(b) CG75-Cr100-6P and CG75-Cr200-8P

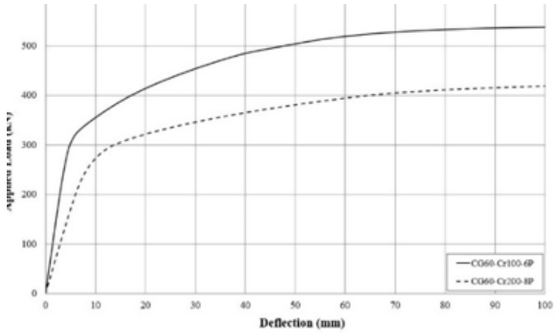

(c) CG60-Cr100-6P and CG60-Cr200-8P

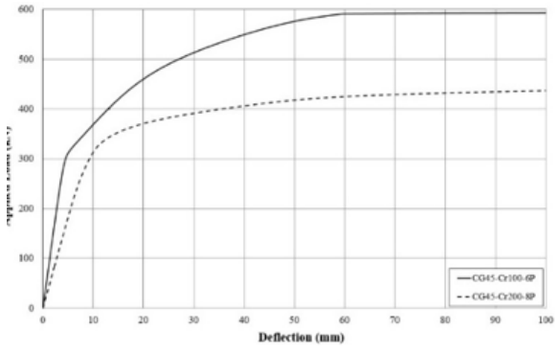

(d) CG45-Cr100-6P and CG45-Cr200-8P

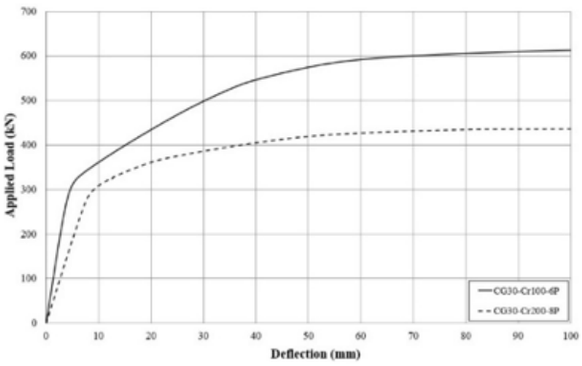

(e) CG30-Cr100-6P and CG30-Cr200-8P

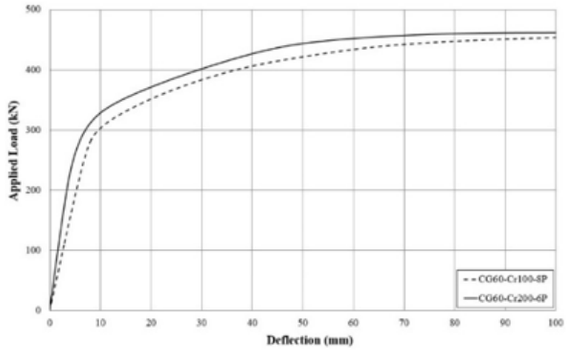

(f) CG60-Cr100-8P and CG60-Cr200-6P

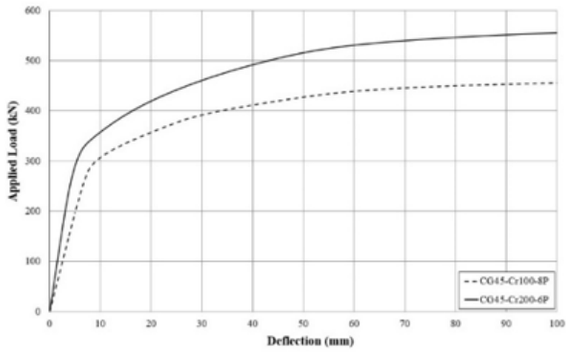

(g) CG45-Cr100-8P and CG45-Cr200-6P

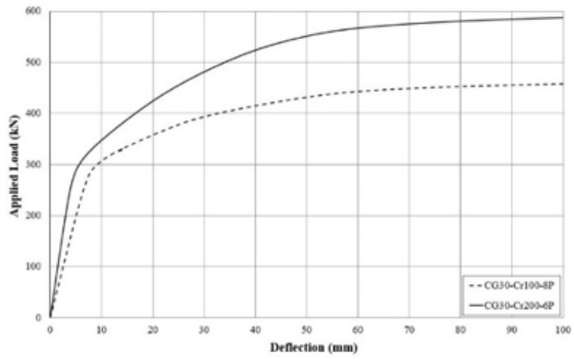

(h) CG30-Cr100-8P and CG30-Cr200-6P

FIGURES 7(a)-(h). The load-deflection response for the composite girders with the same inclination angle, θ, but varying opening sizes, do, and span lengths, L

Even though the opening size may influence the ultimate strength of the composite girder, the composite girder with a 200 mm opening and short span has a higher curve than the girder with a long span. Figures 8(a)-(c) show that the curve for composite girder with a short span have a higher stiffness in the elastic stage, which resulted in a higher ultimate strength compared to the composite girders with a long span and the same opening size. This result indicates that the inclined stiffener contributes to sustain the load-carrying capacity even with a large opening size.

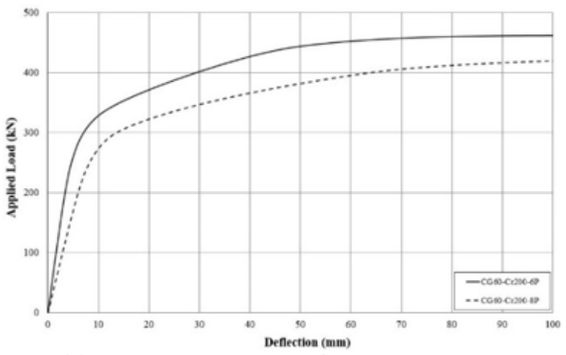

(a) CG60-Cr200-6P and CG60-Cr200-8P

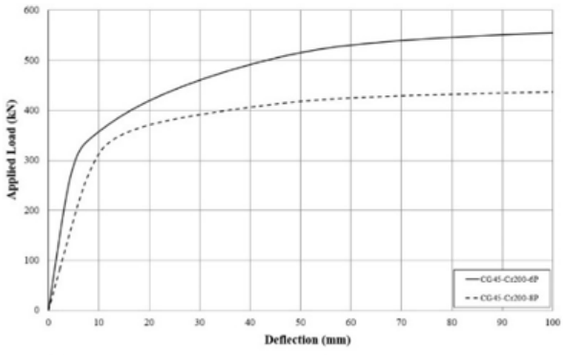

(b) CG45-Cr200-6P and CG45-Cr200-8P

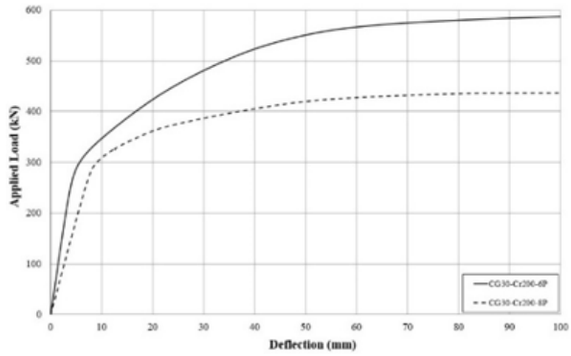

(c) CG30-Cr200-6P and CG30-Cr200-8P

FIGURES 8(a)-(c). The load-deflection response for the composite girders with the same inclination angle, θ, and opening size of 200 mm but varying span lengths, L

The composite girder with a long span and small opening size may benefit from an inclination angle of 90° and 75° compared to the composite girders with a 200 mm opening size and short span because the smaller web opening reduced the tension field action in the web panels slightly. Figures 9(a)-(b) show the load-deflection curves of these models. Figures 10(a) and (b) show a similar trend for the composite girder with the same opening size of 200 mm but a different span length.

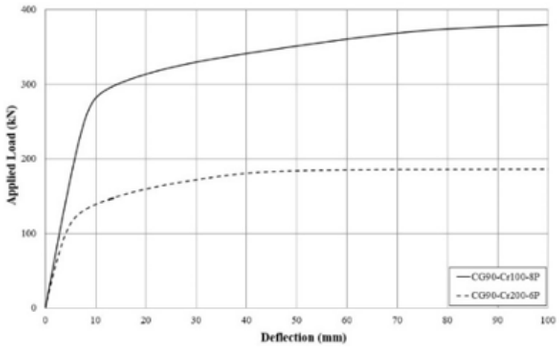

(a) CG90-Cr100-8P and CG90-Cr200-6P

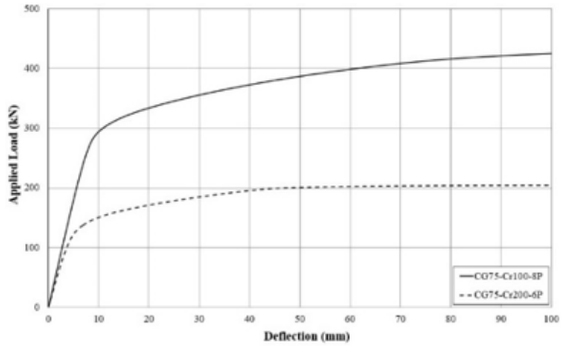

(b) CG75-Cr100-8P and CG75-Cr200-6P

Figures 9(a) and (b). The load-deflection responses for the composite girder with an inclination angle of 90° and 75° but varying opening sizes, do, and span lengths, L.

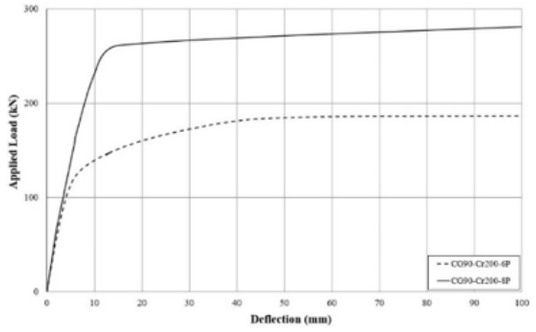

(a) CG90-Cr200-6P and CG90-Cr200-8P

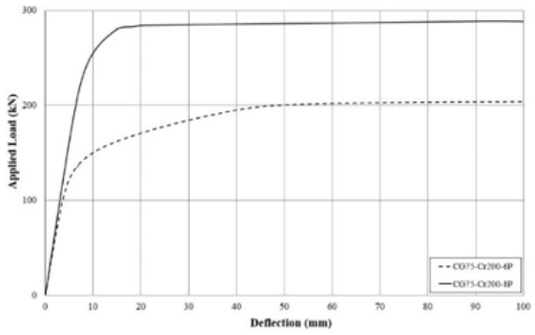

(b) CG75-Cr200-6P and CG75-Cr200-8P

Figures 10(a) and (b). The load-deflection response for the composite girders with the same inclination angle, θ, and opening size, do, but varying span lengths, L

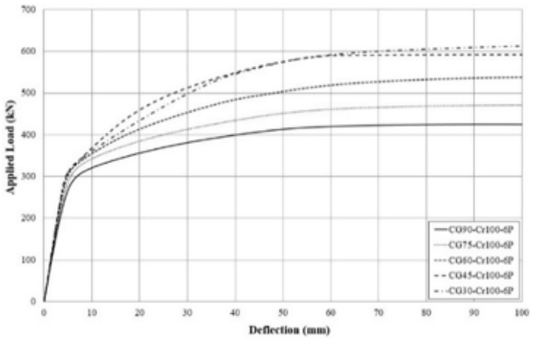

(a) CG90-Cr100-6P, CG75-Cr100-6P, CG60-Cr100-6P, CG45-Cr100-6P and CG30-Cr100-6P

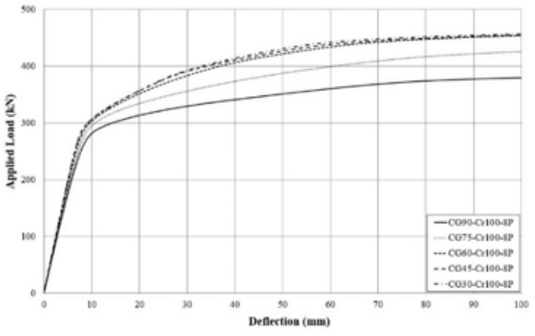

(b) CG90-Cr100-8P, CG75-Cr100-8P, CG60-Cr100-8P, CG45-Cr100-8P and CG30-Cr100-8P

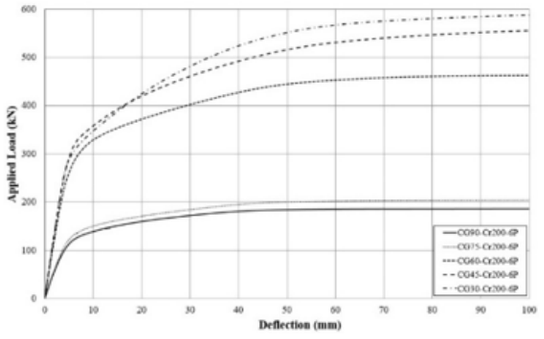

(c) CG90-Cr200-6P, CG75-Cr200-6P, CG60-Cr200-6P, CG45-Cr200-6P and CG30-Cr200-6P

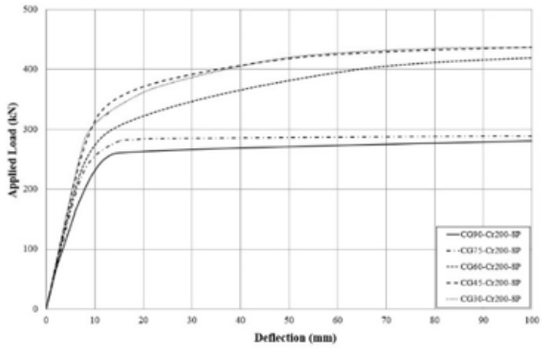

(d) CG90-Cr200-8P, CG75-Cr200-8P, CG60-Cr200-8P, CG45-Cr200-8P and CG30-Cr200-8P.

FIGURES 11(a)-(d). The load-deflection curves for the girders with different inclination angles, θ, but same opening size, do, and span length, L

DEFORMATION BEHAVIOUR

The concentrated point load applied at the mid-span of each finite element model caused a diagonal buckling upon reaching the critical buckling value. All composite girders showed a similar behaviour at the critical loading. The tension membrane sustained the higher loading in the post-buckling stage and delayed the failure until an out-of-plane deformation occurred on the web panels. The vertical deflection increased with higher applied load and exceeded the deflection in the elastic phase due to the higher flexural stiffness.

Figures 12 to 31 show the Von-Mises stress contour and deformation of all girders at the ultimate load. The colour intensity of the stress contour in the middle of the web increased with a smaller inclination angle of the intermediate stiffener, whereas the applied concentrated load produced higher stress intensity at the mid-span of all girders. The plotted contour plot shows that composite girders with an inclined stiffener have a higher compressive strength than those with a vertical stiffener.

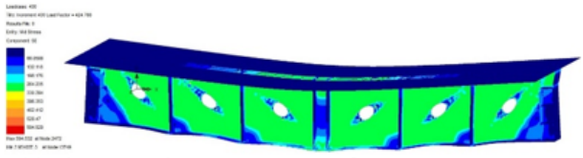

(a) The Von Mises stress contour for CG90-Cr100-6P at the ultimate loading

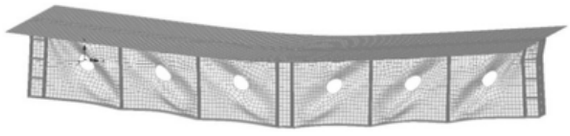

(b) Deformation failure of CG90-Cr100-6P

FIGURES 12(a) and (b). The formation of tension field on the web plate of CG90-Cr100-6P at the ultimate load of $P_{u.FEM}$ = 424.768 kN

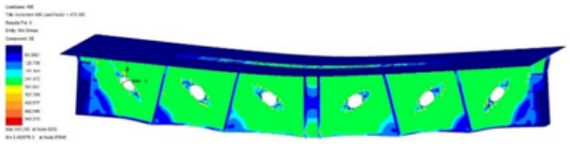

(a) The Von Mises stress contour for CG75-Cr100-6P at the ultimate loading

(b) The deformation failure of CG75-Cr100-6P

FIGURES 13(a) and (b). The formation of tension field on the web plate of CG75-Cr100-6P at the ultimate load of $P_{u.FEM}$ = 470.395 kN

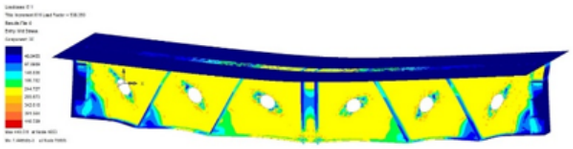

(a) The Von Mises stress contour for CG60-Cr100-6P at the ultimate loading

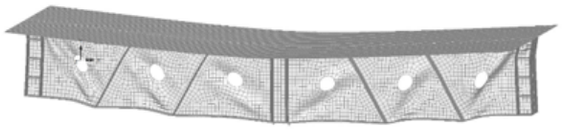

(b) The deformation failure of CG60-Cr100-6P

FIGURES 14(a) and (b). The formation of tension field on the web plate of CG60-Cr100-6P at the ultimate load of $P_{u.FEM}$ = 538.350 kN

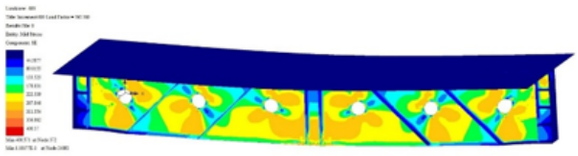

(a) The Von Mises stress contour for CG45-Cr100-6P at the ultimate loading

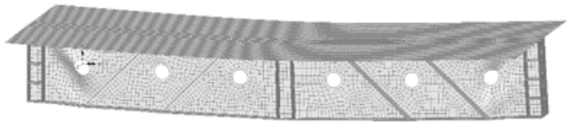

(b) Deformation failure of CG45-Cr100-6P

FIGURES 15(a) and (b). The tension field on the web plate of CG45-Cr100-6P at the ultimate load of $P_{u.FEM}$ = 592.560 kN

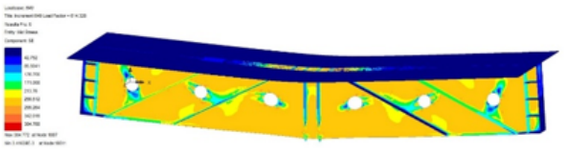

(a) The Von Mises stress contour for CG30-Cr100-6P at the ultimate loading

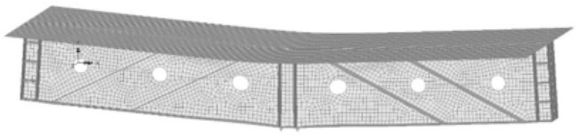

(b) Deformation failure of CG30-Cr100-6P

FIGURES 16(a) and (b). The formation of tension field formation on the web plate of CG30-Cr100-6P at the ultimate load of $P_{u.FEM}$M = 614.328 kN

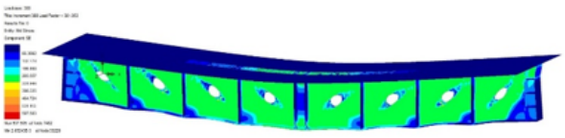

(a) The Von Mises stress contour for CG90-Cr100-8P at the ultimate loading

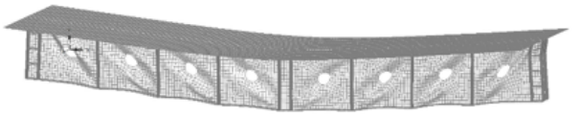

(b) Deformation failure of CG90-Cr100-8P

FIGURES 17(a) and (b). The formation of tension field on the web plate of CG90-Cr100-8P at the ultimate load of $P_{u.FEM}$ = 381.053 kN

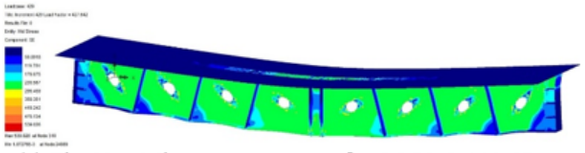

(a) The Von Mises stress contour for CG75-Cr100-8P at the ultimate loading

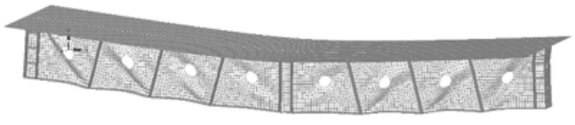

(b) Deformation failure of CG75-Cr100-8P

FIGURES 18(a) and (b). The formation of tension field on the web plate for girder CG75-Cr100-8P at the ultimate load of $P_{u.FEM}$ = 427.642 kN

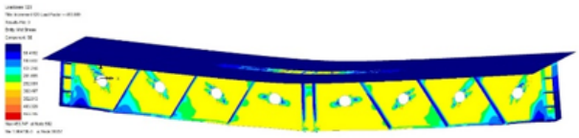

(a) The Von Mises stress contour for CG60-Cr100-8P at the ultimate loading

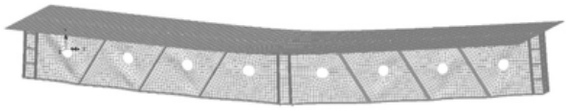

(b) Deformation failure of CG60-Cr100-8P

FIGURE 19(a) and (b). The formation of tension field on the web plate of CG60-Cr100-8P at the ultimate load of $P_{u.FEM}$= 453.989 kN

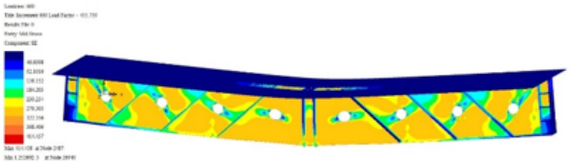

(a) The Von Mises stress contour for CG45-Cr100-8P at the ultimate loading

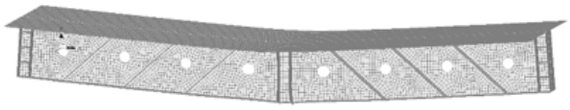

(b) Deformation failure of CG45-Cr100-8P

FIGURES 20(a) and (b). The formation of tension field on the web plate of CG45-Cr100-8P at the ultimate load of $P_{u.FEM}$ = 455.759 kN

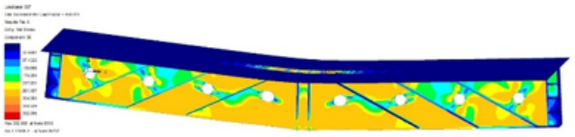

(a) The Von Mises stress contour for CG30-Cr100-8P at the ultimate loading

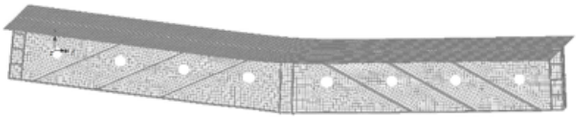

(b) Deformation failure of CG30-Cr100-8P

FIGURES 21(a) and (b). The formation of tension field on the web plate of CG30-Cr100-8P at the ultimate load of $P_{u.FEM}$ = 458.814 kN

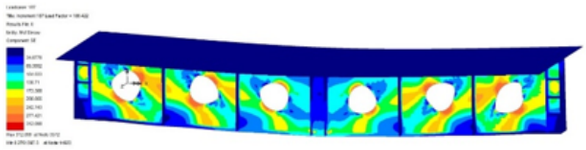

(a) The Von Mises stress contour for CG90-Cr200-6P at the ultimate loading

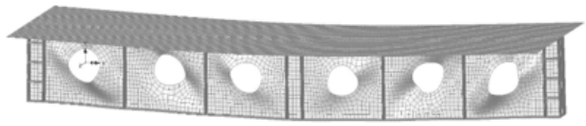

(b) Deformation failure of CG90-Cr200-6P

FIGURES 22(a) and (b). The formation of tension field on the web plate of CG90-Cr200-6P at the ultimate load of $P_{u.FEM}$ = 186.422 kN

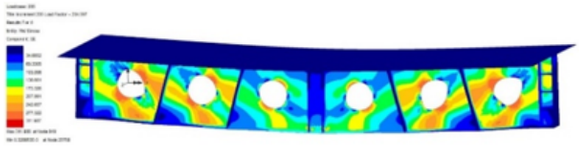

(a) The Von Mises stress contour for CG75-Cr200-6P at the ultimate loading

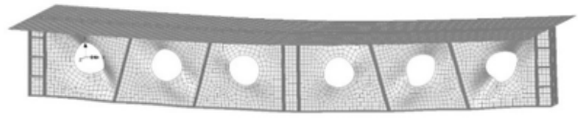

(b) Deformation failure of CG75-Cr200-6P

FIGURES 23(a) and (b). The formation of tension field on the web plate of CG75-Cr200-6P at the ultimate load of $P_{u.FEM}$ = 204.597 kN

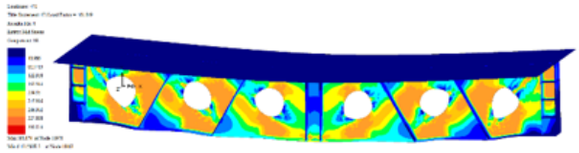

(a) The Von Mises stress contour for CG60-Cr200-6P at the ultimate loading

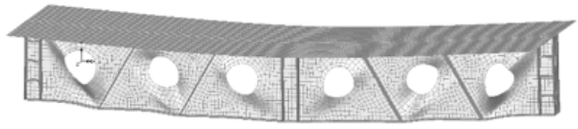

(b) Deformation failure of CG60-Cr200-6P

FIGURES 24(a) and (b). The formation of tension field on the web plate of CG60-Cr200-6P at the ultimate load of $P_{u.FEM}$ = 461.849 kN

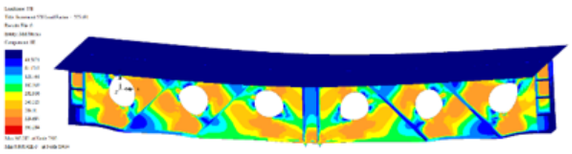

(a) The Von Mises stress contour for CG45-Cr200-6P at the ultimate loading

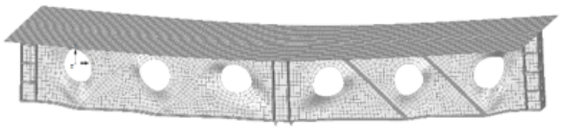

(b) Deformation failure of CG45-Cr200-6P

FIGURES 25(a) and (b). The formation of tension field on the web plate of CG45-Cr200-6P at the ultimate load of $P_{u.FEM}$ = 555.491 kN

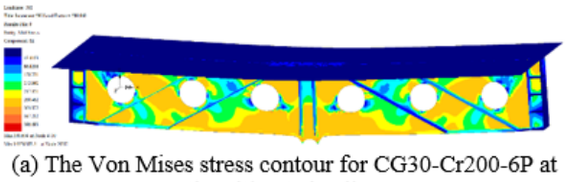

(a) The Von Mises stress contour for CG30-Cr200-6P at the ultimate loading

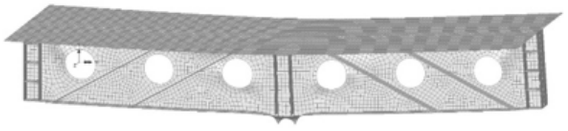

(b) Deformation failure of CG30-Cr200-6P

FIGURES 26(a) and (b). The formation of tension field on the web plate of CG30-Cr200-6P at the ultimate load of $P_{u.FEM}$ = 589.860 kN

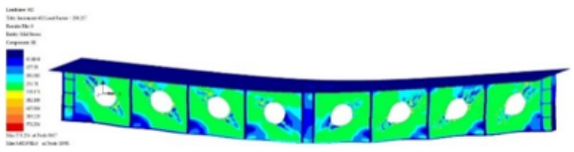

(a) Von Mises stress contour for CG90-Cr200-8P at the ultimate loading

(b) Deformation failure of CG90-Cr200-8P

FIGURES 27(a) and (b). The formation of tension field on the web plate of CG90-Cr200-8P at the ultimate load of $P_{u.FEM}$ = 280.257 kN

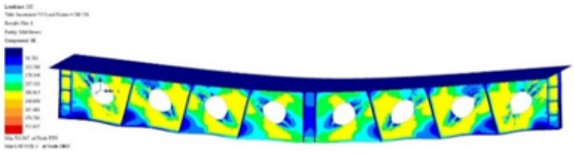

(a) The Von Mises stress contour for CG75-Cr200-8P at the ultimate loading

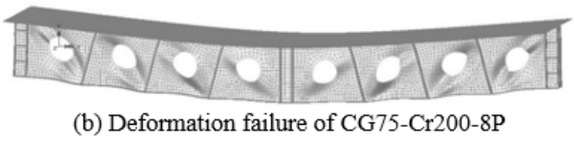

(b) Deformation failure of CG75-Cr200-8P

FIGURES 28(a) and (b). The formation of tension field on the web plate of CG75-Cr200-8P at the ultimate load of $P_{u.FEM}$ = 288.538 kN

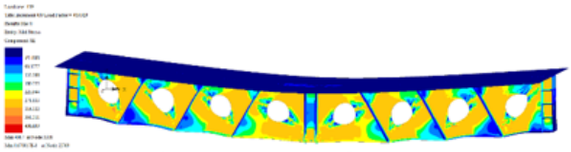

(a) The Von Mises stress contour for CG60-Cr200-8P at the ultimate loading

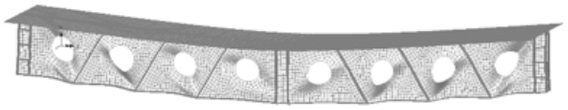

(b) Deformation failure for girder CG60-Cr200-8P

FIGURES 29(a) and (b). The formation of tension field on the web plate of CG60-Cr200-8P at the ultimate load of $P_{u.FEM}$ = 419.929 kN

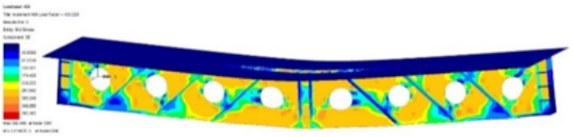

(a) The Von Mises stress contour for CG45-Cr200-8P at the ultimate loading

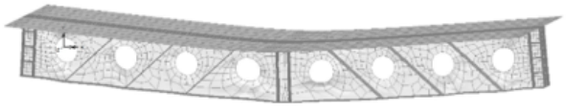

(b) Deformation failure of CG45-Cr200-8P

FIGURES 30(a) and (b). The formation of tension field on the web plate of CG45-Cr200-8P at the ultimate load of $P_{u.FEM}$ = 433.228 kN

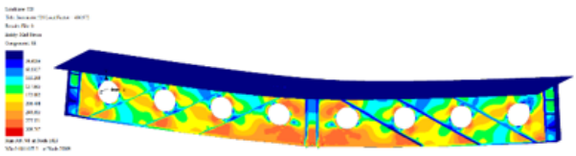

(a) The Von Mises stress contour for CG30-Cr200-8P at the ultimate loading

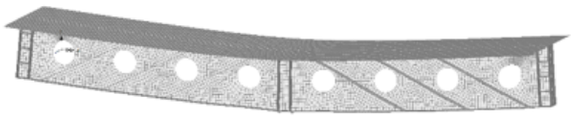

(b) Deformation failure of CG30-Cr200-8P

FIGURES 31(a) and (b). The formation of tension field on web plate of CG30-Cr200-8P at the ultimate load of $P_{u.FEM}$ = 436.972 kN

CONCLUSION

This research performed a non-linear finite element analysis on the simply supported perforated composite girders with inclined intermediate stiffener imposed with a combination of shear action and moment action. The results showed varying ultimate strength and behaviour at the failure of the composite girders. The parametric study considered the inclination angle of the intermediate stiffener, θ, opening size, d_o, and span length, L. Reducing the angle from 90° to 30° gave the perforated composite girders a higher ultimate load-carrying capacity.

The inclined stiffener restored the shear-loading capacity lost due to the opening on the composite girder, including the composite girders with a long span. The composite action sustained the exerted load at an early stage and delayed the failure. This preliminary study has provided general insights on the ultimate load behaviour of composite girders with inclined stiffeners. Future research should perform a more in-depth analysis of the stiffeners with an inclination angle of less than 30° and consider other parameters. Additionally, experimental investigation and detailed theoretical works are strongly recommended for this study to provide insight into the behaviour of the perforated composite girder with inclined stiffener.

ACKNOWLEDMENT

This research is supported by research grant Geran Galakan Penyelidik Muda (GGPM-2019-053). The authors wish to thank the Department of Civil Engineering, Universiti Kebangsaan Malaysia, for providing the facilities to carry out this research.

DECLARATION OF COMPETING INTEREST

None.

REFERENCES

Alinia, M. M. & Moosavi, S. H. 2008. A parametric study on the longitudinal stiffeners of web panels. *Thin-Walled Structures* 46(11): 1213–1223.

Azmi, M. R., Yatim, M. Y. M., Badaruzzaman, W. H. W. & Ahmad, I. K. 2017. Tests on plate girders containing web openings and inclined stiffeners. *International Journal of Applied Engineering Research* 12(6): 1075–1083.

Basher, M. A., Shanmugam, N. E. & Khalim, A. R. 2009. Web openings in horizontally curved composite plate girders. *Journal of Constructional Steel Research* 65(8–9): 1694–1704.

Baskar, K. & Shanmugam, N. E. 2003. Steel-concrete composite plate girders subject to combined shear and bending. *Journal of Constructional Steel Research* 59(4): 531–557.

Darehshouri, S.F., Shanmugam, N.E. & Osman, S.A. 2013. An analytical method for ultimate shear strength of composite plate girders with web openings. *Engineering Structures* 56: 610–620.

Ellobody, E. 2017. Interaction of buckling modes in railway plate girder steel bridges. *Thin-Walled Structures* 115: 58–75.

Evans, H. R., Porter, D. M. & Rockey, K. C. 1978. The Collapse Behaviour of Plate Girders subjected to Shear and Bending. IABSE Proceedings P-18/78.

Gavare, P.R. & Patil, P.S.N. 2018. Parametric Study of Plate Girder Using Different Stiffener Arrangement. *International Journal of Advance Research in Science and Engineering*: 1161–1174.

Guarnieri, G. 1985. Collapse of Plate Girders with inclined stiffeners, *Journal of Structural Engineer. ASCE* 111(2): 378-399.

M. Y. M. Yatim, M. R. Azmi, L. Y. Ling, M. A. P. A. Agus and N. F. N. Sazali. 2017. Ultimate Load Behaviour of Perforated Steel Plate Girders with Inclined Stiffeners. *Jurnal Kejuruteraan – Isu Khas* I: 47–55.

Pritykin, A. I. & Kirillov, I. E. 2015. Critical rigidity of stiffener for increasing shear stability of rectangular plate. *Mechanika* 21(3): 174–179.

Xiao, Y., Xue, X.Y., Sun, F.F. & Li, G.Q. 2018. Postbuckling shear capacity of high-strength steel plate girders. *Journal of Constructional Steel Research* 150: 475–490.

Yatim, M. Y. M., Shanmugam, N. E. & Wan Badaruzzaman, W. H. 2015. Tests of partially connected composite plate girders. *Thin-Walled Structures* 91: 13–28.

Yuan, H. X., Chen, X. W., Theofanous, M., Wu, Y. W., Cao, T. Y. & Du, X. X. 2019. Shear behaviour and design of diagonally stiffened stainless steel plate girders. *Journal of Constructional Steel Research* 153: 588–602.

Yatim, M. Y. M., M. R. Azmi & M. Mukhlisin. 2020. Performance of Steel Plate Girders with Inclined Stiffeners. *Jurnal Kejuruteraan* 32(3): 129-137.